Scanning flow-impedance microscopy: A simple imaging technique based on hydrodynamics

Tae Young Kim,[1] Dong-Kwon Kim,[2] and Sung Jin Kim[1,a)]
[1]*School of Mechanical, Aerospace and Systems Engineering, Korea Advanced Institute of Science and Technology, Daejeon 305-701, Republic of Korea*
[2]*Department of Mechanical Engineering, Ajou University, Suwon 443-749, Republic of Korea*

(Received 17 April 2009; accepted 5 September 2009; published online 1 October 2009)

We introduce the concept of scanning flow-impedance microscopy (SFIM) which is an imaging technique based on hydrodynamics. Using a simple experimental setup including a mass flow controller and a manometer, the operating principle of SFIM is validated under atmospheric pressure and temperature conditions. Experimental results show that the flow impedance strongly depends on the relative distance between a probe and a specimen. SFIM micrographs of microscale patterns with various linewidths are presented. © *2009 American Institute of Physics.*
[doi:10.1063/1.3238483]

I. INTRODUCTION

Since the scanning tunneling microscope was introduced by Binnig and Rohrer,[1] scanning probe microscopes (SPMs) have attracted considerable attention as a means of studying surfaces. Thus far, various SPMs (Refs. 2–7) have been suggested based on different physical principles and used in different research areas according to their own merits.

The scanning flow-impedance microscope (SFIM) (Ref. 8) proposed in the present study is a sort of scanning probe microscope based on hydrodynamics. As a probe microscope, the SFIM has some advantages. In the SFIM, specimens can be observed in any gas or liquid under atmospheric pressure and temperature conditions, unlike an electron microscope[9–11] which requires specimens be in a partial vacuum. The resolution of the SFIM is not limited by the diffraction of light or electrons but by the size of the probe. As a new type of probe microscope, the SFIM has some advantages. The use of some earlier SPMs was limited by the material properties of a specimen, working environments, and operating conditions. The scanning ion-conductance microscope (SICM) is applicable only when the surrounding fluid is electrically conductive and has a constant electrical conductivity.[12] For the contact type of atomic force microscope (AFM), damage or contamination of the specimen during the scanning process can be a significant problem. Therefore, it is important to scan the specimen in the noncontact mode of the AFM, which is a nondestructive surface imaging technique.[13,14] In the case of heterogeneous surfaces such as semiconductors, some SPMs need cumbersome composite processes after scanning the surface several times under different scanning conditions.[9] On the other hand, the SFIM is free from these drawbacks: it can image the topography regardless of the surface heterogeneity or the electromagnetic properties of the specimen and working fluid without touching the surface.

The advantage of the SFIM also comes from its wide applicability. Applications of the SFIM would include surface fabrication,[15] electronics cooling,[16] or surface coating[17] by means of an impinging jet from the aperture of the probe. The intensity of the flow stream used for fabrication and coating processes can be controlled by varying the flow rate or the distance between the probe and the surface. The SFIM also can be used as tweezers for small particles, such as biomolecules, by collecting or releasing them through the aperture of the probe using a suction or blowing type pump.

II. OPERATING PRINCIPLE AND FEATURES OF THE SFIM

The operating principle of the SFIM is based on hydrodynamic phenomena. As the name implies, the SFIM can image the surface topography of a specimen by measuring the flow impedance variation that strongly depends on the probe-to-specimen distance. When the fluid flow issuing from the aperture of the probe impinges on the specimen surface, the surface affects the flow stream. As the distance between the surface and the probe shrinks to a certain point, which is termed "set point" in this study, the surface begins to act as a resistance to the flow stream. As a result, the pressure needed to drive the fluid flow with the fixed average velocity u through the probe also increases. The difference between probe tip pressure and the ambient pressure (Δp_l), an index of the flow impedance variation, is given as[18]

$$\frac{\Delta p_l}{\frac{1}{2}\rho u^2} = f\left(\frac{\rho u D_i}{\mu}, \frac{z}{D_i}\right), \tag{1}$$

where ρ, μ, u, and D_i are the density of the fluid, the viscosity of the fluid, the average stream velocity at the probe tip, and the ID of the probe, respectively. When the fluid properties, the ID of the probe, and the average stream velocity are fixed, the pressure difference would only be a function of the probe-to-specimen vertical distance (z). Consequently, flow impedance data obtained by scanning the probe over the specimen can be converted into the topographical informa-

a)Author to whom correspondence should be addressed. Tel.: +82-42-350-3043. FAX: +82-42-350-8207. Electronic mail: sungjinkim@kaist.ac.kr.

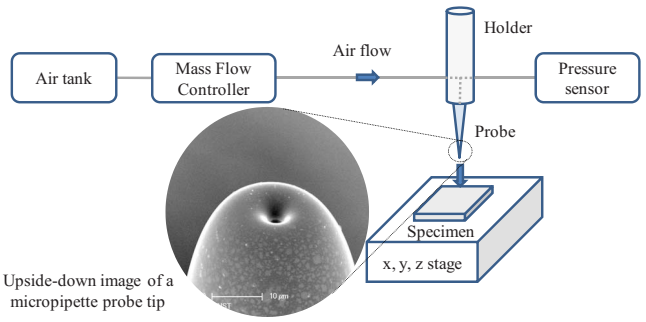

FIG. 1. (Color online) Schematic diagram of the experimental setup. A syringe pump, instead of the gas tank and the mass flow controller, can be used when a liquid is used as a working fluid.

tion of the specimen. In this manner, the SFIM based on the hydrodynamic phenomena can image the specimen surface.

III. EXPERIMENTS

Experiments were performed under atmospheric pressure and temperature conditions to demonstrate the concept of the SFIM. An attractive feature of the SFIM lies in its simple experimental setup. Figure 1 shows the schematic diagram of the experimental setup. Air was used as a working fluid. A mass flow controller (Brooks Inc.) was used for precise control of the stream velocity of the air. A micromanometer (FCO510, Furness-Controls Ltd.) measured the difference between the internal pressure of the probe and the ambient pressure. Essentially, micropipette probes were fabricated using a micropipette puller (P-2000, Sutter Instrument Com.) and a microforge (Narishige Scientific Instruments Laboratory) as shown in Figs. 2(a)–2(d). In addition to the pulled micropipette probes, probes made of aluminum alloy 6063 with millimeter-scale diameters were also fabricated as shown in Figs. 2(e) and 2(f). An *xyz* stage (Suruga Seiki), actuated by stepper motors with a resolution of 50 nm and positional accuracy within 10 μm, was used in moving a test specimen. All experimental apparatuses were set on an optical table with an air damping system to measure the physical quantities under vibration isolation. The photograph of the experimental setup is shown in Fig. 3.

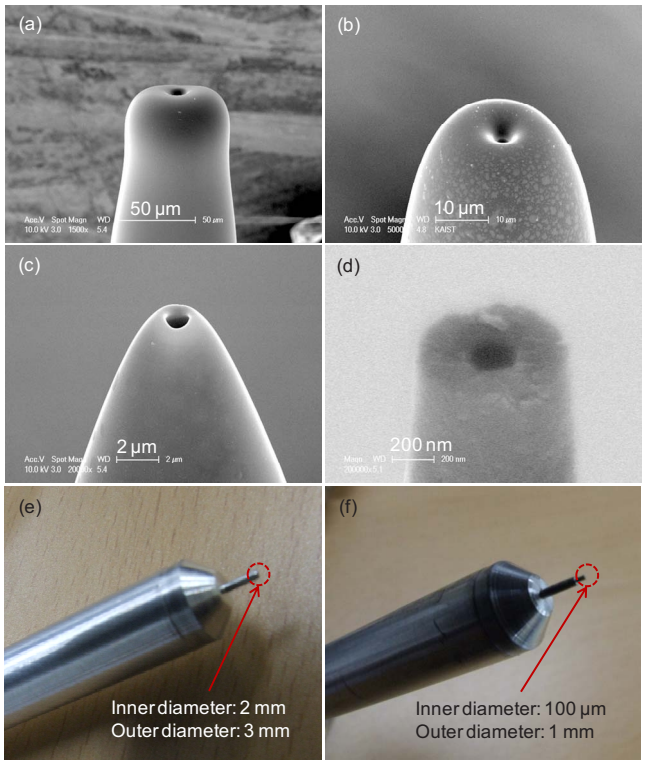

FIG. 2. (Color online) [(a)–(d)] SEM images of pulled micropipette probes. IDs of the pipette probes are in the range of 200 nm–15 μm. [(e) and (f)] Photographs of aluminum probes. IDs of the aluminum probes are 100 μm and 2 mm.

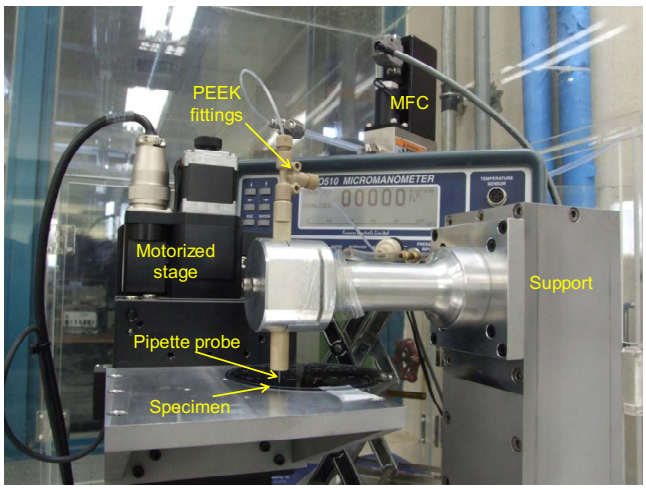

FIG. 3. (Color online) Photograph of the experimental setup.

To examine the dependence of the flow impedance characteristic on the probe-to-specimen vertical distance, distance-flow impedance curves in the SFIM were experimentally obtained. By moving the surface away the probe incrementally, the steady-state values of the pressure difference were obtained. The reference pressure is the internal gauge pressure of the probe when the surface moves far from the probe and the surface no longer affects the flow stream. Table I shows the values of the reference pressure for each experimental case.

IV. RESULTS AND DISCUSSION

Figure 4 presents the experimentally obtained distance-flow impedance curves. The vertical axis shown in Fig. 4 represents the difference between the internal gauge pressure of the probe and the reference pressure. To find the dependence of the flow impedance on the probe-to-specimen distance regardless of the probe's length, the reference pressure

TABLE I. Reference pressures for each experimental case.

Aluminum probe (2 mm ID and 3 mm OD)			
Mass flow rate (SCCM)	100	200	300
P_{ref} (Pa)	410	890	1520
Aluminum probe (100 μm ID and 1 mm OD)			
Mass flow rate (SCCM)	1	2	3
P_{ref} (Pa)	79	160	248

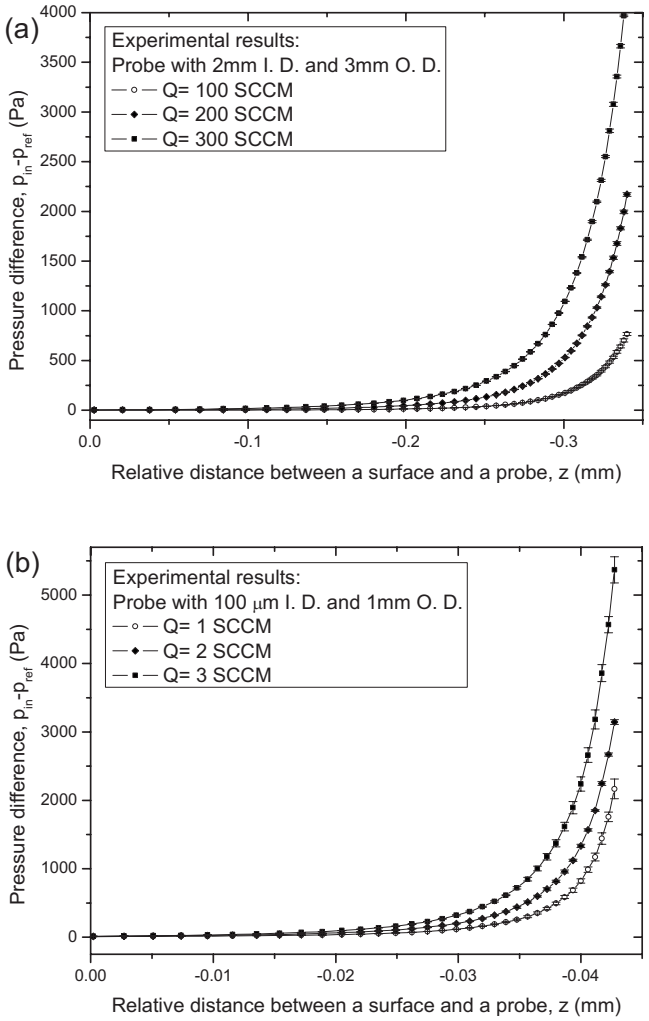

FIG. 4. Experimental results for distance-flow impedance curves.

values are subtracted from the gauge pressure values. The horizontal axis in Fig. 4 shows the relative distance between the probe and the surface. Only the relative distance variation between the probe and the surface is specified in the SFIM. The set point at which the pressure difference begins to vary from the reference pressure starts at a greater distance from the surface at a higher flow rate issuing from the probe. Accordingly, operation range of the SFIM increases with the flow rate. When the surface approaches the probe beyond the set point, the pressure difference exponentially increases. The region between the set point and the surface of the specimen is termed "operating region" in the present study. One thing that must be addressed is that the sensitivity of the SFIM, the flow impedance variation according to the distance variation, increases as the flow rate flowing through the probe increases. Thus, features of the SFIM that set it apart from other SPMs are that its operating range and sensitivity can be controlled by varying the flow rate of the fluid passing through the aperture of the probe. In an open loop mode (constant-height mode), these distance-flow impedance curves are used to convert the flow impedance data into the topographical information of the specimen.

A two-dimensional scan was performed using an aluminum probe with an inner diameter (ID) of 100 μm and an

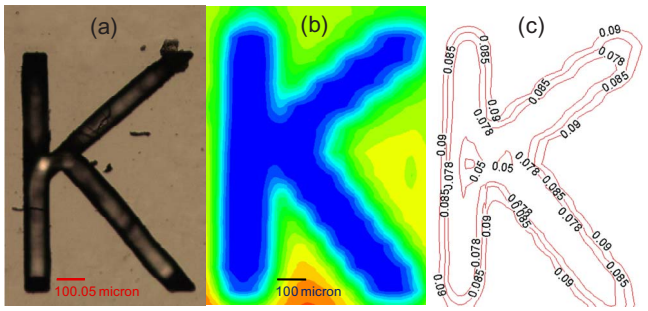

FIG. 5. (Color online) Two-dimensional scan results obtained using an aluminum probe with an ID of 100 μm and an OD of 1 mm (a) Optical image of the pattern with 100 μm line width. (b) SFIM micrograph. (c) Contour lines (unit: mm).

outer diameter (OD) of 1 mm. In the experiment, the topography of the specimen was obtained under the constant-height mode for convenience. The test specimen has microscale patterns of various sizes created on a silicon wafer by a dry etching process. The scanned image is a structure that appears as the letter "K" with a minimum feature size of approximately 100 μm. Figure 5(a) is the picture of the pattern obtained using an optical microscope (Olympus TH4–200). The scan result obtained using the SFIM is shown in Fig. 5(b). Comparison of results between the optical microscope and the SFIM shows that the SFIM can discern the pattern. After applying the distance-flow impedance curve to the SFIM result, contour lines of the pattern could be obtained as shown in Fig. 5(c). The contour lines show that the depth of the pattern is approximately 90 μm that is comparable to 110 μm, the result of a surface profiling system (SIS-1200, SNU precision).

The SFIM yields the distorted image if the ID of the probe is larger than the feature size of the tested patterns. As shown in Figs. 6(a)–6(c), the SFIM micrograph of the pattern ambiguously reproduces the optical image of the pattern. Even though the depth of the pattern predicted by the SFIM is 90 μm and is not significantly different from the result by surface profiling system, the measured linewidth of the pattern is magnified to the size of the ID of the probe.

Another two-dimensional scan was performed to confirm the effect of the probe size on the lateral resolution of the SFIM. Patterned structures with a minimum feature size of 30 μm were used as test specimens. A micropipette with an ID of approximately 15 μm, which is shown in Fig. 2(a), was used as a probe. Figure 7(b) shows that a reproduced

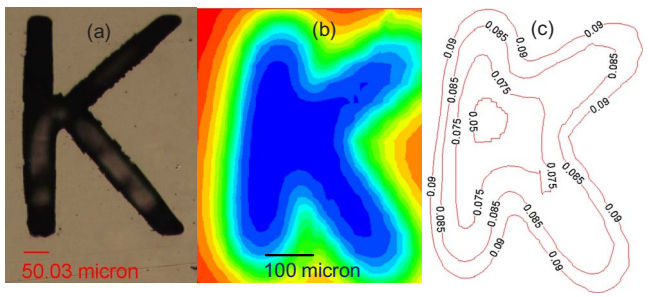

FIG. 6. (Color online) Distorted images obtained using an aluminum probe with an ID of 100 μm and an OD of 1 mm. (a) Optical image of the pattern with 50 μm linewidth. (b) SFIM micrograph. (c) Contour lines (unit: mm).

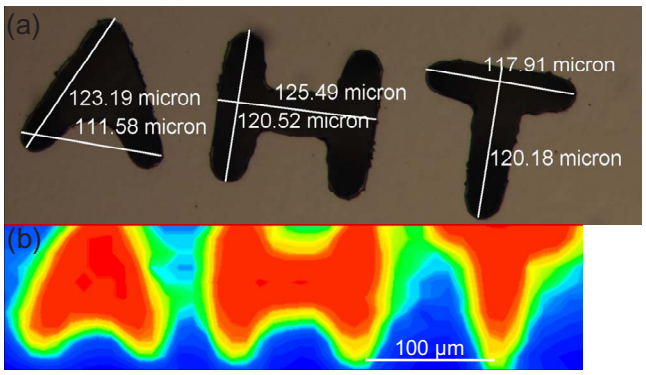

FIG. 7. (Color online) Effect of the probe size on the resolution of the SFIM. (a) Optical image of the pattern with 30 μm linewidth. (b) Two-dimensional SFIM micrograph obtained using a pulled micropipette probe with an ID of 15 μm.

image obtained by scanning the probe over the test specimen. Compared to the result obtained by the optical microscope, shown in Fig. 7(a), the outlines of the test specimen are well reproduced by the SFIM. Therefore, based on the experimental results presented in Figs. 6 and 7, it can be noted that the lateral resolution of the SFIM depends on the probe size, especially on the ID of the probe. It appears that the effect of the OD on the resolution is not significant. The resolution of the SFIM can be enhanced by reducing the size of the ID of the probe. The SFIM can image the topography of a specimen precisely when the ID of the probe is smaller than the minimum feature size of the patterns. The distance-flow impedance curves and the two-dimensional scan results imply that SFIM, which is based on hydrodynamic phenomena, can be used as an imaging technique.

The resolution of the SFIM is mainly dependent on two aspects. One of these is the size of the probe tip. Based on the experimental results, the ID of the probe should be smaller than the smallest feature size of the patterns in order to exactly reproduce the shapes of patterns on the surface. Thus, the pipette probes shown in Figs. 2(b)–2(d) should be used in discerning the shape of a pattern when the minimum feature size of the pattern is smaller than 5 μm. In addition, the smallest size of the micropipette tip diameter can be reduced to 10 nm as reported by Brown and Flaming.[19] The second aspect of the resolution of the SFIM is the accuracy of the stage used to move the test specimen. Most SPMs use the piezoelectric actuator system for extremely high resolution.[20–22] However, in the present study, a stage with microstepper motors with an accuracy of several micrometers was used as an actuator to move the specimen. Accordingly, using a piezoelectric actuator, the ultimate resolution of the SFIM can be enhanced up to several tens of nanometers, the resolution of the near-field scanning optical microscope (NSOM) or the SICM which uses a micropipette as a probe.[12,23]

The constant pressure mode (or the closed-loop mode) can be used for the SFIM to discern the height variation in a specimen. In this mode, the measured pressure difference is used as a feedback signal to maintain the probe-to-surface distance at a predetermined constant value in the operating range. The locus of the z stage supporting the test specimen directly reflects the topography of the specimen's surface. The SFIM was operated in the constant pressure mode, and the experimental results have shown that the SFIM can image the surface topography of the specimen in the constant pressure mode.

In conclusion, we have described the concept of SFIM, a simple imaging technique which is based on hydrodynamics. Using a simple experimental setup, we have experimentally validated the operating principle of the SFIM and studied the dependence of the resolution on the probe size. SFIM micrographs of microscale patterns with various line widths created on the silicon wafer are presented.

This work was supported by the Korea Science and Engineering Foundation (KOSEF) through the National Research Laboratory. Program funded by the Ministry of Education, Science and Technology (Grant No. M10600000224O6J000022410). This work was also supported by the new faculty research fund of Ajou University.

APPENDIX: DEVELOPMENT OF AN EMPIRICAL MODEL FOR DISTANCE-FLOW IMPEDANCE CURVES AND DISCUSSION ON THE SENSITIVITY AND THE VERTICAL RESOLUTION OF THE SFIM

In this section, we explain how an empirical model for distance-flow impedance curves can be obtained. Based on the proposed model, the sensitivity and the vertical resolution of the SFIM are discussed.

In this study, an empirical model for the distance-flow impedance curves is developed. As mentioned in the results and discussion section, the set point means a point at which the difference between the internal pressure of the probe and the ambient pressure begins to vary from the reference pressure. The difference between the internal gage pressure of the probe and the reference pressure at the set point is termed "set point pressure." The set point pressure value is empirically defined as a function of the Reynolds number and the ID of the probe.

$$p_{\mathrm{sp}} = \frac{\mathrm{Re}^{0.55}}{D_i^{0.15}}. \tag{A1}$$

Since the distance-flow impedance curves exponentially increase with decreasing probe-to-specimen distance in the operating region, the empirical model has an exponential form. The two exponential functions are combined using the composite solution technique[24]

$$\frac{\Delta p_l''}{1/2\rho u^2} = \{[a\exp(bz^*)]^n + [c\exp(dz^*)]^n\}^{1/n} = f(\mathrm{Re}, z^*), \tag{A2}$$

where $\Delta p_l'' = p_{\mathrm{in}} - p_{\mathrm{ref}} - p_{\mathrm{sp}}$, $\mathrm{Re} = \rho u D_i/\mu$, and $z^* = z/D_i$. The set point is the origin of dimensionless probe-to-specimen distance z^*.

The two exponential functions in Eq. (A2) are the two asymptotes. The combination parameter n is used to control the behavior of the model in the transition region between the asymptotes. Four empirical coefficients a, b, c, d, and the combination parameter n are determined as follows:

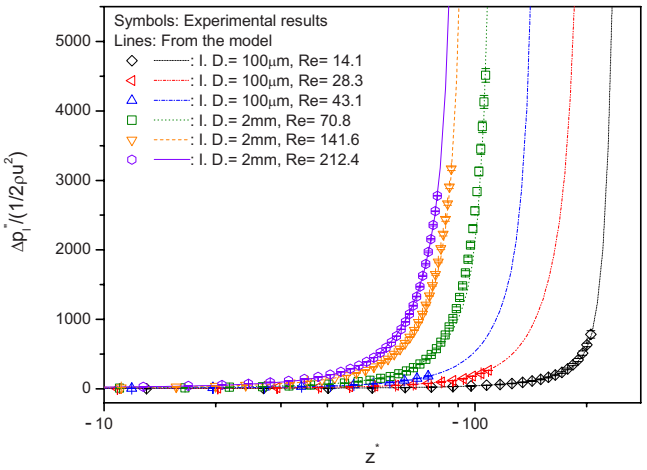

FIG. 8. (Color online) Validation of the proposed model.

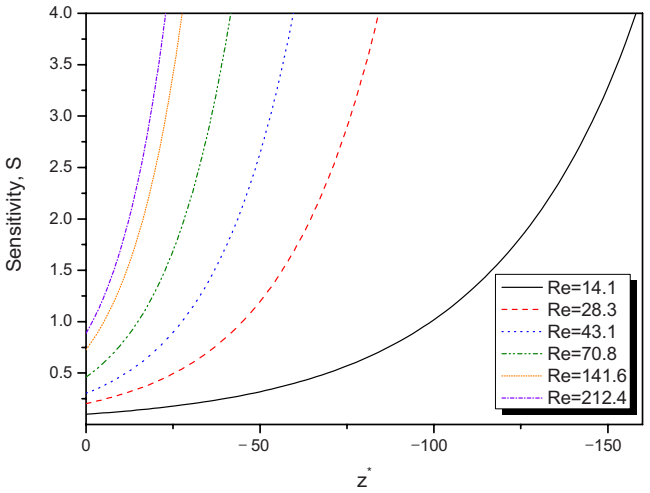

FIG. 9. (Color online) Sensitivity of the SFIM.

$$a = 2.467 + \frac{17.09\ \mathrm{Re}}{117.615 + \mathrm{Re}},$$

$$b = 1.148 \times 10^{-3} + \frac{0.075\ \mathrm{Re}}{33.788 + \mathrm{Re}},$$

$$c = 10.18 \times 10^{-6} + \frac{125.86 \times 10^{-6}\ \mathrm{Re}}{21.744 + \mathrm{Re}},$$

$$d = 9.678 \times 10^{-3} + \frac{0.223\ \mathrm{Re}}{32.01 + \mathrm{Re}},$$

$$n = 2.$$

For the validation of the model, the results from the model are compared with experimental results. As shown in Fig. 8, the results from the model are in good agreement with the experimental data.

The empirical model can be used to convert the flow-impedance data into the topographical information of the specimen and to study the sensitivity and the vertical resolution of the SFIM. The pumping power needed to generate an impinging jet through a nozzle can be also calculated using the model. If the shape of the impinging jet nozzle and the flow rate of the fluid are given, the pumping power can be determined by obtaining the pressure drop value from the model.

Using the proposed model, the sensitivity and the vertical resolution of the SFIM are also studied. The sensitivity is one of the most important parameters of probe microscopes. If the sensitivity is smaller than the resolution of the pressure sensor, the SFIM cannot recognize the topographical variation in the specimen and thus the SFIM cannot be used for surface imaging. The sensitivity of the SFIM is the derivative of the flow-impedance variation with respect to the dimensionless distance z^* and is given as

$$S(z^*) = \frac{\partial[\Delta p_i''/(1/2\rho u^2)]}{\partial z^*} = \{[a\ \exp(bz^*)]^2 + [c\ \exp(dz^*)]^2\}^{-1/2} \times [a^2 b\ \exp^2(bz^*) + c^2 d\ \exp^2(dz^*)]. \quad \text{(A3)}$$

When the Reynolds number is fixed, the sensitivity of the SFIM, $S(z^*)$, increases with decreasing dimensionless distance z^*, as shown in Fig. 9. The SFIM has the minimum sensitivity at the set point, where $z^*=0$, and the sensitivity at the set point is given as

$$S(0) = \left.\frac{\partial[\Delta p_i''/(1/2\rho u^2)]}{\partial z^*}\right|_{z^*=0} = \frac{a^2 b + c^2 d}{\sqrt{a^2 + c^2}}. \quad \text{(A4)}$$

If the operating conditions are substituted into Eq. (A4), we have Eq. (A5).

$$S(0) \times \mathrm{Re}^2 > \frac{2\rho D_i^3}{\mu^2}\left(\frac{R_p}{h}\right), \quad \text{(A5)}$$

where h and R_p are the minimum height variation in the specimen and the resolution of the pressure sensor, respectively. The inequality sign is used in Eq. (A5) because the sensitivity of the SFIM should be larger than the resolution of the pressure sensor. Equation (A5) is the requirement to be satisfied to reproduce the surface topography of the specimen. The left hand side of Eq. (A5) is only a function of the Reynolds number. Thus the Reynolds number should be properly determined based on the operating conditions such as the minimum height variation in the specimen, the resolution of the pressure sensor, and the ID of the probe.

The vertical resolution of the SFIM can be obtained by rearranging Eq. (A5) with respect to h.

$$h > \frac{2\rho D_i^3 R_p}{(\mu\ \mathrm{Re})^2 S(0)}. \quad \text{(A6)}$$

The SFIM cannot reproduce the height variation in a specimen which is smaller than the right hand side of Eq. (A6). In other words, under given working conditions, the minimum value of h that follows Eq. (A6) is the vertical resolution of the SFIM. The vertical resolution of the SFIM also depends on the Reynolds number. Higher vertical resolution of the SFIM can be obtained by increasing the Reynolds number.

[1] G. Binnig and H. Rohrer, Helv. Phys. Acta **55**, 726 (1982).
[2] G. Binnig, C. F. Quate, and Ch. Gerber, Phys. Rev. Lett. **56**, 930 (1986).
[3] B. Rogers, D. York, N. Whisman, M. Jones, K. Murray, J. D. Adams, T. Sulchek, and S. C. Minne, Rev. Sci. Instrum. **73**, 3242 (2002).

[4] F. Giannazzo, F. Priolo, V. Raineri, and V. Privitera, Appl. Phys. Lett. **76**, 2565 (2000).
[5] A. Majumdar, J. P. Carrejo, and J. Lai, Appl. Phys. Lett. **62**, 2501 (1993).
[6] M. Wilms, M. Kruft, G. Bermes, and K. Wandelt, Rev. Sci. Instrum. **70**, 3641 (1999).
[7] R. C. Reddick, R. J. Warmack, D. W. Chilcott, S. L. Sharp, and T. L. Ferrell, Rev. Sci. Instrum. **61**, 3669 (1990).
[8] S. J. Kim, T. Y. Kim, and D.-K. Kim, Korean Patent No. 10–2008–0119103 (2008).
[9] H. K. Wickramasinghe, Sci. Am. **260**, 98 (1989).
[10] G. P. Lopez, H. A. Biebuyck, and G. M. Whitesides, Langmuir **9**, 1513 (1993).
[11] M. Hammar, F. K. LeGoues, J. Tersoff, M. C. Reuter, and R. M. Tromp, Surf. Sci. **349**, 129 (1996).
[12] P. K. Hansma, V. B. Elings, O. Marti, and C. E. Bracker, Science **242**, 209 (1988); C. B. Prater, P. K. Hansma, M. Tortonese, and C. F. Quate, Rev. Sci. Instrum. **62**, 2634 (1991).
[13] R. Garcia and R. Perez, Surf. Sci. Rep. **47**, 197 (2002).
[14] W. A. Hofer, A. S. Foster, and A. L. Shluger, Rev. Mod. Phys. **75**, 1287 (2003).
[15] X. Ding, Y. Li, D. Wang, and Q. Yin, Ceram. Int. **30**, 1885 (2004).
[16] Y. Mitsutake and M. Monde, Heat Mass Transfer **37**, 321 (2001).
[17] A. Arzate and P. A. Tanguy, Chem. Eng. Res. Des. **83**, 111 (2005).
[18] I. E. Idelchik, *Handbook of Hydraulic Resistance*, 3rd ed. (CRC, Boca Raton, FL, 2000).
[19] K. T. Brown and D. G. Flaming, *Advanced Micropipette Techniques for Cell Physiology* (Wiley, New York, 1986).
[20] J. M. Paros and L. Weisbord, Mach. Des. **37**, 151 (1965).
[21] G. C. Joyce and G. C. Wilson, J. Phys. E: J. Sci. Instrum. **2**, 661 (1969).
[22] R. D. Deslattes, Appl. Phys. Lett. **15**, 386 (1969).
[23] W.-S. Chang, J. Kim, S.-H. Cho, and K.-H. Whang, Jpn. J. Appl. Phys., Part 1 **45**, 2082 (2006).
[24] S. W. Churchill and R. Usagi, AIChE J. **18**, 1121 (1972).